Contrib Mineral Petrol (2006) 151: 615–630
DOI 10.1007/s00410-006-0077-4

ORIGINAL PAPER

Blair Schoene · Samuel A. Bowring

U–Pb systematics of the McClure Mountain syenite: thermochronological constraints on the age of the $^{40}Ar/^{39}Ar$ standard MMhb

Received: 3 November 2005 / Accepted: 16 February 2006 / Published online: 22 March 2006

Abstract Recent advances in U–Pb geochronology allow unprecedented levels of precision in the determination of geological ages. However, increased precision has also illuminated the importance of understanding subtle sources of open-system behavior such as Pb-loss, inheritance, intermediate daughter product disequilibria, and the accuracy of the model assumptions for initial Pb. Deconvolution of these effects allows a much richer understanding of the power and limitations of U–Pb geochronology and thermochronology. In this study, we report high-precision ID-TIMS U–Pb data from zircon, baddelleyite, titanite and apatite from the McClure Mountain syenite, from which the $^{40}Ar/^{39}Ar$ hornblende standard MMhb is derived. We find that excess ^{206}Pb in zircon due to inclusions of high-Th minerals and elevated Th/U in titanite and apatite jeopardize the utility of the ^{238}U–^{206}Pb system in this rock. Strongly air-abraded zircons give dates that are younger than chemical-abraded zircons, which yield a statistically robust $^{207}Pb/^{235}U$ date of 523.98 ± 0.12 Ma that is interpreted as the crystallization age. We explore the best method of Pb_c correction in titanite and apatite by analyzing the U–Pb isotopes of K-feldspar and using 2-D and 3-D regression methods—the latter of which yields the best results in each case. However, the calculated compositions of Pb_c for titanite, apatite and K-feldspar are different, implying that using a single Pb_c correction for multiple U–Pb thermochronometers may be inaccurate. The U–Pb thermochronological results are used to predict a closure time for Ar in hornblende of 522.98 ± 1.00 Ma. Widely cited K–Ar and $^{40}Ar/^{39}Ar$ dates overlap with the U–Pb date, and relatively large errors make it impossible to verify whether U–Pb dates are systematically $\leq 1\%$ older than K–Ar and $^{40}Ar/^{39}Ar$ dates.

Communicated by T. L. Grove

B. Schoene (✉) · S. A. Bowring
Department of Earth, Atmospheric and Planetary Sciences,
Massachusetts Institute of Technology, Room 54-1116,
77 Massachusetts Ave., Cambridge, MA 02139, USA
E-mail: schoene@mit.edu
Tel.: +1-617-2530844
Fax: +1-617-2536735

Introduction

U–Pb geochronology is one of the most precise methods for placing temporal constraints on igneous and metamorphic processes and for establishing benchmarks for the stratigraphic timescale. Because of the high closure temperature ($T_c \geq 1{,}000$°C) for diffusion of Pb and the high U (and negligible initial Pb) concentrations in zircon, this mineral is ideal for dating the timing of crystallization under igneous and metamorphic conditions. In addition, minerals with lower T_c such as titanite ($T_c \approx 550$–650°C; Cherniak 1993; Corfu 1988; Frost et al. 2000), apatite ($T_c \approx 450$–550°C; Chamberlain and Bowring 2000; Cherniak et al. 1991; Nemchin and Pidgeon 1999) and rutile ($T_c \approx 400$–500°C; Cherniak and Watson 2000; Mezger et al. 1991; Schmitz and Bowring 2003) have allowed the determination of thermal histories of rocks in the lower to middle crust. Over the past 15 years, improvements in isotope dilution thermal ionization mass-spectrometry (ID-TIMS), sample preparation, and laboratory blanks have resulted in internal precision on individual dates to below the 0.1% level, allowing for the calibration of geologic time at an unprecedented level. However, such precision has also revealed the importance of quantitatively addressing what are often subtle sources of open-system behavior in U–Pb systematics such as intermediate daughter product disequilibria, Pb-loss, and inheritance (see reviews in Hanchar and Hoskin 2003). These issues are also important in U–Pb thermochronology, though precision is often limited by relatively low ratios of radiogenic lead to initial (a.k.a. common) lead (Pb^*/Pb_c), introducing significant error in the correction for the isotopic composition of Pb_c (Ludwig 1980, 1998). In fact, the Pb_c correction is arguably the most prominent source of

inaccuracy in U–Pb thermochronology and is a critical aspect of calculating dates which are as accurate as they are precise (Chamberlain and Bowring 2000; Corfu 1988; Verts et al. 1996). But because the isotopic signature of Pb in rocks or magmas may vary widely as a function of time and space during crystallization and cooling, each approach to the correction involves a set of assumptions that are difficult to address in detail.

Improvements in both the precision and accuracy of U–Pb geo- and thermochronology is important not only for a better understanding of the geologic record but also for the purposes of intercalibrating the U–Pb system with other geochronologic methods. For example, Renne et al. (1998a) pointed out that many $^{40}Ar/^{39}Ar$ dates are systematically younger than U–Pb dates by $\leq 1\%$, and Min et al. (2000) suggested—based on a re-evalution of the experimental data—that this is because the values of the ^{40}K decay constant used by the geochronologic community (Steiger and Jäger 1977) should be ~2% lower and that larger associated uncertainties are more realistic. Because high-precision experimental redetermination of the ^{40}K decay constant is a very difficult task, it has been suggested that it be calibrated against the U decay constants, whose values are the most precisely known in geochronology (Jaffey et al. 1971). However, Mattinson (2000) and Schoene et al. (2006) use systematic discordance of high-precision ID-TIMS U–Pb dates to show that one or both of the mean values of the U decay constants are inaccurate (but within the reported errors), which will adversely affect the approach of calibrating other decay schemes against U–Pb. Intercalibration of the two methods therefore requires both the generation of a large set of mineral pairs dated with high precision by both methods that unambiguously record the same event, and ultimately repeated experiments to redetermine the U and K decay constants.

Intercalibrating the U–Pb and $^{40}Ar/^{39}Ar$ systems is complicated in part by the contrasting closure temperatures of diffusion of the respective daughter products (Dodson 1973). High-K minerals used in $^{40}Ar/^{39}Ar$ geochronology such as hornblende ($T_c \approx 550$–$500°C$; Harrison 1981) or micas ($T_c < 350°C$; Grove and Harrison 1996; Harrison et al. 1985) record cooling through their closure temperatures and therefore cannot necessarily be compared with zircon U–Pb dates that record crystallization. This problem may be overcome by using $^{40}Ar/^{39}Ar$ geochronology in sanidine from young volcanic rocks, whose $^{40}Ar/^{39}Ar$ systematics likely record the timing of eruption because the T_c is below that of magmatic temperatures. However, U–Pb dates from zircons in young magmatic systems are sometimes complicated by pre-eruptive crystallization of unknown duration (Reid and Coath 2000; Reid et al. 1997; Schmitz and Bowring 2001). This problem becomes less important as the age of the sample increases because reasonable estimates of magma residence time (Reid and Coath 2000; Reid et al. 1997) are likely to be smaller than the individual errors of high-precision U–Pb dates. On the other hand, older volcanic rocks pose difficulty for $^{40}Ar/^{39}Ar$ dating because mineralogically pure sanidine is unstable at surface conditions and may not record the timing of eruption (e.g., Min et al. 2000). Quickly cooled plutonic rocks provide another option for intercalibration, though assessing systematic biases between U–Pb and $^{40}Ar/^{39}Ar$ dates introduced by ^{40}K decay constant inaccuracies is necessarily based on an assumed cooling rate, unless U–Pb thermochronology can be used to establish a thermal context for the $^{40}Ar/^{39}Ar$ data (Schmitz and Bowring 2001; Schoene et al. 2006).

In this contribution, we address the issues of precision versus accuracy in U–Pb dating and systematic biases between the U–Pb and $^{40}Ar/^{39}Ar$ dating methods. We present data from the McClure Mountain syenite, the source of a widely used standard in $^{40}Ar/^{39}Ar$ dating, the McClure Mountain hornblende (MMhb; Alexander et al. 1978; Samson and Alexander 1987). Ample K–Ar and $^{40}Ar/^{39}Ar$ data for this hornblende allow for the assessment of interlaboratory bias and sample heterogeneity. In addition, the abundance of high-U minerals such as zircon, baddeleyite, titanite, and apatite allow us to characterize the thermal history of this rock in the U–Pb system alone. Back-scattered electron (BSE) and cathodoluminesence (CL) imaging in combination with ID-TIMS U–Pb dating of zircon provide a high-precision date for crystallization of the rock. Careful assessment of the compositions of Pb_c in titanite, apatite and K-feldspar in relation to their petrographic context allows us to calculate a temperature–time curve with high confidence, providing a framework for comparison with $^{40}Ar/^{39}Ar$ dates. In addition, assessment of Pb isotopic systematics as a function of time allows for the construction of petrologic models for the McClure Mountain magmatic system.

Methods

Electron microprobe analysis

The MIT JEOL 733 Superprobe electron microprobe (EMP) facility was used for both imaging and energy dispersive spectrometry (EDS) of zircon separates and thin sections. Zircons were hand-picked based on varying morphology, color, clarity and degree of metamictization, and were mounted in epoxy resin and polished to reveal the crystal centers. Both grain-mounts and thin sections were polished, cleaned and carbon-coated. BSE and CL images were collected using a 15 keV accelerating voltage with a beam current between 4 and 50 nA depending on the individual mineral. EDS analysis was conducted using a 1 μm beam size, and this technique was used for mineral identification and qualitative major element analysis.

U–Pb analytical procedure

Minerals were extracted from the rock sample by standard crushing, Wilfley table, heavy-liquid, and magnetic

separation. Zircon fractions were pre-treated with either the air-abrasion (Krogh 1982) or chemical-abrasion (Mattinson 2003, 2005) technique. Air-abraded zircons were ultrasonically cleaned in 30% HNO_3 for 1 h, fluxed in 30% HNO_3 at ~80°C for 1 h, and rinsed in ultrapure acetone and H_2O before being loaded into 300 µl Teflon FEP microcapsules and spiked with a mixed ^{233}U–^{235}U–^{205}Pb tracer. Zircon was dissolved in ~120 µl 29 M HF with ~25 µl 30% HNO_3 at ~210°C for 48 h, dried to fluorides, and then re-dissolved in 6 M HCl at ~180°C overnight. For the chemical-abrasion technique, zircons were placed in a muffle furnace at 900 ± 20°C for ~60 h in quartz beakers before being transferred to 300 µl Teflon FEP microcapsules and leached in ~120 µl 29 M HF + ~25 µl 30% HNO_3 for 12–14 h at ~180°C. Fractions were then rinsed in ultrapure H_2O, fluxed on a hotplate at ~80°C for an hour in 6 M HCl, ultrasonically cleaned for 1 h, placed back on the hotplate for an additional 30 min, and rinsed in ultrapure H_2O and 30% HNO_3. Fractions were then spiked and fully dissolved using the procedure described above. Cleaning and dissolution of baddeleyite, titanite and feldspar follow that of air-abraded zircons; apatite was rinsed only in water and dissolved in 12 N HCl overnight. Step-wise leaching of feldspar followed the procedure of Housh and Bowring (1991), modified to account for smaller sample size. U and Pb were separated using an HCl-based single-column (zircon and baddeleyite) or an HBr-based two-column (titanite, apatite, feldspar, and feldspar leachates) anion exchange chemistry modified after Krogh (1973).

U and Pb isotopic measurements were done on a VG Sector-54 multi-collector thermal-ionization mass spectrometer at MIT. Pb and U were either loaded together (HCl-based chemistry) or separate (HBr-based chemistry) on Re filaments in a silica-gel/phosphoric acid mixture (Gerstenberger and Haase 1997). Pb was measured by either (1) peak-hopping on a single Daly detector (for smaller beams); (2) a dynamic Faraday–Daly routine (F–D) that cycles between placing mass 204 in the axial Daly collector and masses 205–208 on the H1–H4 Faraday detectors to placing mass 205 in the axial Daly and masses 206–208 in the H1–H3 Faradays, providing real-time Daly gain correction; or (3) for samples with large 204 peaks, in static Faraday mode. U isotopic measurements were made as the oxide in static Faraday mode. Mass fractionation and detector bias on the Daly detector were determined to be 0.25 ± 0.04%/amu over a wide temperature range based on analysis of the NBS-981 common Pb standard and spiked aliquots of NBS-983. Mass fractionation on the F–D and static Faraday routines was determined to be 0.07 ± 0.04%/amu. U mass fractionation was calculated in real-time using a ^{233}U–^{235}U double spike. All common Pb for the zircon and baddeleyite analyses was attributed to procedural blank. A sensitivity test shows that the composition of the common Pb in zircon and baddeleyite has little or no effect on the calculated dates. Total procedural Pb blanks for the HBr-based chemistry were determined to be 1.5 ± 0.4 pg, which was used in the reduction of titanite, apatite, and total dissolution K-feldspar data. K-feldspar leachates were assigned a Pb blank of 10 pg based on the amount of reagent used in the procedure, and the blank is a negligible proportion of the total Pb in those analyses. U blanks are difficult to measure, but are ≤ 0.1 pg, and only in feldspar analyses is the blank a significant portion of the total U, but in no cases are the blank-corrected isotopic ratios sensitive to the U blank. All samples were spiked with a ^{205}Pb–^{233}U–^{235}U tracer, whose calibration is detailed in Schoene et al. (2006), in which an error of ±0.015% is assigned to the Pb/U of the tracer.

Isotopic ratios and associated errors were reduced using the algorithms of Ludwig (1980) and are presented at the 95% confidence level. Tracer and decay constant errors are considered systematic errors and are added to the error of weighted mean data clusters (Ludwig 1998; Mattinson 1987; Renne et al. 1998b; Schmitz and Bowring 2001; Schmitz et al. 2003). Values and errors for the uranium decay constants are from Jaffey et al. (1971). Concordia plots, isochron regressions and weighted mean calculations and associated MSWD (mean square of weighted deviates; York 1969) calculations were generated in ISOPLOT (Ludwig 1991).

Sample description

The sample used in this study is from the McClure Mountain complex, a series of ultramafic to low-Si alkalic igneous intrusions in the Wet Mountains region of Colorado, USA. The complex is composed of early crystallized mafic-ultramafic layered intrusions such as olivine gabbro, pyroxenite, anorthosite and dunite, which are in turn intruded by massive hornblende–biotite syenite and then by nepheline syenite (Parker and Hildebrand 1963; Shawe and Parker 1967). A series of carbonatites, lamprophyres, and quartz–barite–thorite dikes and veins crosscuts these older units (Olson et al. 1977).

This study focuses on the hornblende-biotite syenite from which MMhb was extracted (Alexander et al. 1978). A re-collection of the syenite (D. Hawkins, personal communication, 1998) attempted to sample the same quarry-derived boulders as were described in Alexander et al. (1978). Major constituent minerals include K-feldspar, plagioclase, hornblende, biotite and clinopyroxene. Titanite and apatite make up several percent of the rock. Nepheline, magnetite, ilmenite, zircon, baddeleyite, zirconolite, calcite, iron-sulfides, and alteration products such as sericite and chlorite constitute < 2% of the rock. Hornblende, pyroxene, biotite, titanite and apatite occur as ~2–8 mm diameter clusters of intergrown crystals encased in a matrix of microperthitic K-feldspar and plagioclase crystals < 1–10 mm in diameter (Fig. 1a). The rock description of Alexander et al. (1978) did not identify pyroxene in their sample, but instead describes the

hornblende as zoned with olive-green cores and brown-green exteriors. Our thin sections show similar zonation, though the olive-green cores are Mg-rich clinopyroxene (Fig. 1a). In addition to pyroxene cores, hornblende is ubiquitously filled with inclusions of all other phases in the rock, which sometimes occur as euhedral crystals and sometimes filling cracks and cleavages (especially with respect to biotite). In each thin section, there are discrete sub-linear zones several millimeters in length containing calcite, nepheline, baddelleyite and symplectitic plagioclase/K-feldspar intergrowths in addition to other major phases (Fig. 1b). These low-Si, high-CO_2 zones are not located along cracks or in zones of obvious alteration, but instead appear to be concentrated in-between major phase minerals.

Apatite occurs as euhedral crystals ~50–200 μm in diameter and is included in every major phase in the rock, indicating it was an early liquidus phase (Fig. 1a). CL images of apatite in thin section are generally featureless, though some show weak concentric zoning (Fig. 2a). Titanite occurs with hornblende, oxides, and/or biotite as both anhedral and euhedral phenocrysts up to 300 μm in diameter (Figs. 1a, 2b). Zircon ($ZrSiO_4$), baddeleyite (ZrO_2), and zirconolite ($CaZrTi_2O_7$) are rare in thin section, though all were identified in at least one section using EDS. Several ~20 μm zircon grains were identified in thin section by EDS and were located both in clusters with titanite and apatite and also within the feldspar matrix. Traditional mineral separation provided a large amount of zircon, whose textures and geochronology are described in the U-Pb isotopic results section. Baddeleyite is found in both the calcite-rich zones described above (Fig. 2c) and also intergrown with zircon and zirconolite. Zirconolite is also found as microcrystic intergrowths with ilmenite, magnetite and titanite. Though zirconolite has proved useful as a U–Pb geochronometer (Rasmussen and Fletcher 2004), grains found in thin section are <20 μm in diameter and were not recovered in mineral separates.

U–Pb isotopic results

Zircon

Zircon from this sample forms two end-member populations, both of which range in grain-size from 30 to 500 μm. Group 1: magnetic, euhedral, brown-gray dipyramids that are cloudy to opaque due to inclusions and/or metamictization. Group 2: non-magnetic, sub- to anhedral, pink to colorless, translucent grains. These two populations are equally easy to distinguish by CL images (Fig. 3). Note that zircons located in thin section are too small to make generalizations about the petrogrpahic context of the endmember populations identified in mineral separates. Group 1 exhibits both oscillatory growth zoning, typical of magmatic zircons, and "convolute" zoning—a texture that has been interpreted to reflect subsolidus remobilization of trace elements—creating chaotically patchy zones of bright and dim luminesence (Fig. 3d–i; Corfu et al. 2003; Pidgeon et al. 1998). Also, this group of zircons has a higher concentration of inclusions, including anorthite, K-feldspar, magnetite, allanite and thorite (Fig. 3e, g). Allanite inclusions typically contain weight-percent U and Th, and form radiation halos of dim CL about 10–20 μm in radius in the surrounding zircon (Fig. 3g, h). Group 2 zircons are dominated by oscillatory growth zoning, though thin zones of bright or dark luminescence cross-cutting this zonation occur as well; zircon resorption during periods of undersaturation either in the magma or during sub-solidus fluid migration may explain the truncated zonation (Fig. 3a–d).

Seventeen single-grain zircon fractions were analyzed for U–Pb systematics including six group 2 air-abraded grains, one unabraded group 2 zircon, five chemical-abraded group 1 zircons, and five chemical-abraded group 2 zircons. U–Pb isotopic data are presented in Table 1 and a concordia diagram is shown in Fig. 4. All

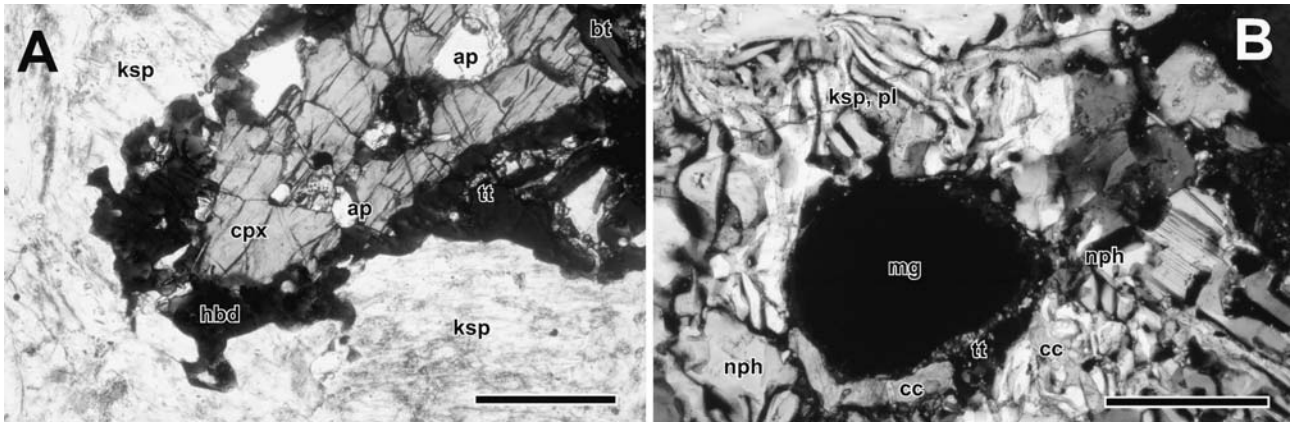

Fig. 1 Photomicrographs from the McClure Mountain syenite. Abbreviations are as follows: *ap* apatite; *bt* biotite; *cc* calcite; *cpx* high-Mg clinopyroxene; *hbd* hornblende; *ksp* K-feldspar; *mg* magnetite; *nph* nepheline; *pl* plagioclase; *tt* titanite. **a** Textural relationship between major constituent minerals. See text for discussion. *Scale bar* is 500 μm. **b** Example of carbonate-rich zone featuring symplectitic intergrowth of plagioclase and K-feldspar, as well as nepheline and calcite. See text for discussion. *Scale bar* is 200 μm

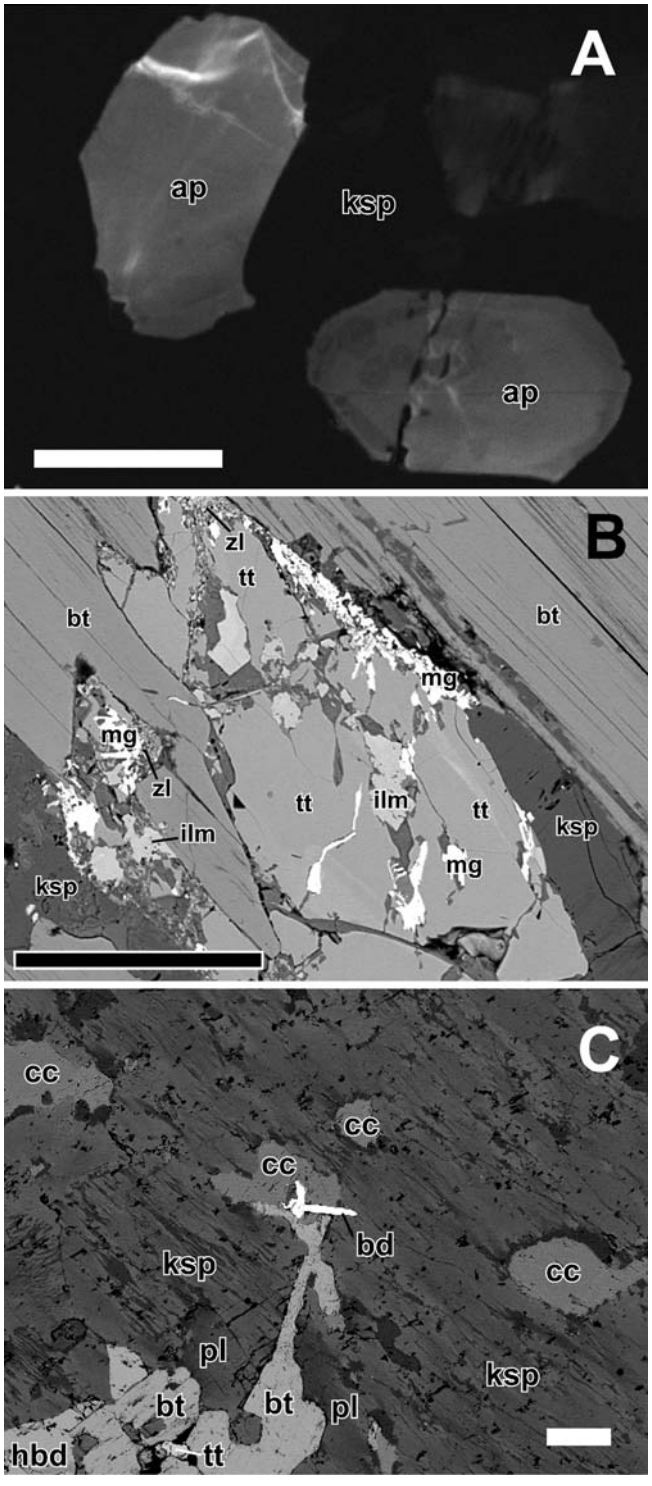

Fig. 2 BSE and CL images. *Scale bar* in each image is 100 μm. All abbreviations are the same as in Fig. 1 with the addition of: *bd* baddelleyite; *ilm* ilmenite; *zl* zirconolite. **a** CL image of sub- to euhedral apatite in K-feldpsar matrix in polished thin section. Note weak concentric zoning in the *right-hand* grain. **b** BSE image depicting typical setting of an inclusion-rich subhedral titanite. Note intergrowths of magnetite, ilmenite, titanite and zirconolite along grain boundaries. **c** BSE image showing baddeleyite spatially associated with calcite. See text for discussion

air-abraded zircons are positively discordant, and yield $^{206}Pb/^{238}U$ and $^{207}Pb/^{235}U$ ratios that are lower than those of the chemical-abraded grains, consistent with Pb-loss in domains that were not totally removed by the air-abrasion technique. The ten chemical-abraded zircons give a range of $^{206}Pb/^{238}U$ dates, and those with the highest Th/U ratios (between 14 and 211; Table 1) are negatively discordant. The dispersion in those data is most likely due to ^{230}Th disequilbrium resulting in excess ^{206}Pb derived from variably abundant inclusions of thorite and allanite in group 1 zircons, as seen in BSE images (Fig. 3e, g). Though previously documented examples of ^{230}Th disequilibrium are interpreted to result from magmatic growth (Mattinson 1973; Parrish 1990; Schärer 1984)—as opposed to Th-rich inclusions—the resulting negative discordance is expected to be similar. Indeed, some group 2 zircons have Th/U above 1 as well, which may be derived from unseen micro-inclusions of high Th minerals or from within the zircon crystal structure. $^{207}Pb/^{235}U$ ratios from all ten of the chemical-abraded zircons are statistically indistinguishable and yield a weighted mean date of $523.98 \pm 0.12/0.18/0.74$ Ma (MSWD = 1.4; internal errors/with tracer calibration errors/with tracer calibration and decay constant errors). We consider this to represent most accurately the crystallization age of the rock.

Baddeleyite

Baddeleyite grains are brown to colorless and range in size from < 20–200 μm. Three clear baddeleyite grains were analyzed (b12, b14 and b15), and these all have low Pb^*/Pb_c (< 15) and two of them are greater than 14% negatively discordant and one plots near concordia (b12). Eleven brown baddeleyites were analyzed, and five are between 3 and 28% negatively discordant while the other fractions span a range of time slightly below concordia from ~520 to 525 Ma (Table 1; Fig. 5). Fraction b8 is more discordant and has an older $^{207}Pb/^{206}Pb$ date than the other five brown grains, which may be due to inheritance (though inheritance is not commonly reported in baddelleyite) or to its relatively low Pb^*/Pb_c (~14). The dispersion of the six grains near concordia is consistent both with continuous growth of baddeleyite and with open-system behavior with respect to U and/or Pb after a single-stage of crystallization. The observed negative discordance in numerous grains provides ample evidence that open-system behavior was important in these grains, and therefore we question whether any of the grains record accurate age information. Four fractions, however, are equivalent (MSWD of equivalence = 1.2) and yield a weighted mean $^{207}Pb/^{235}U$ date of $522.41 \pm 0.27/0.34/1.03$ Ma (MSWD = 0.9; internal errors/with tracer calibration error/with tracer calibration and decay constant error), though

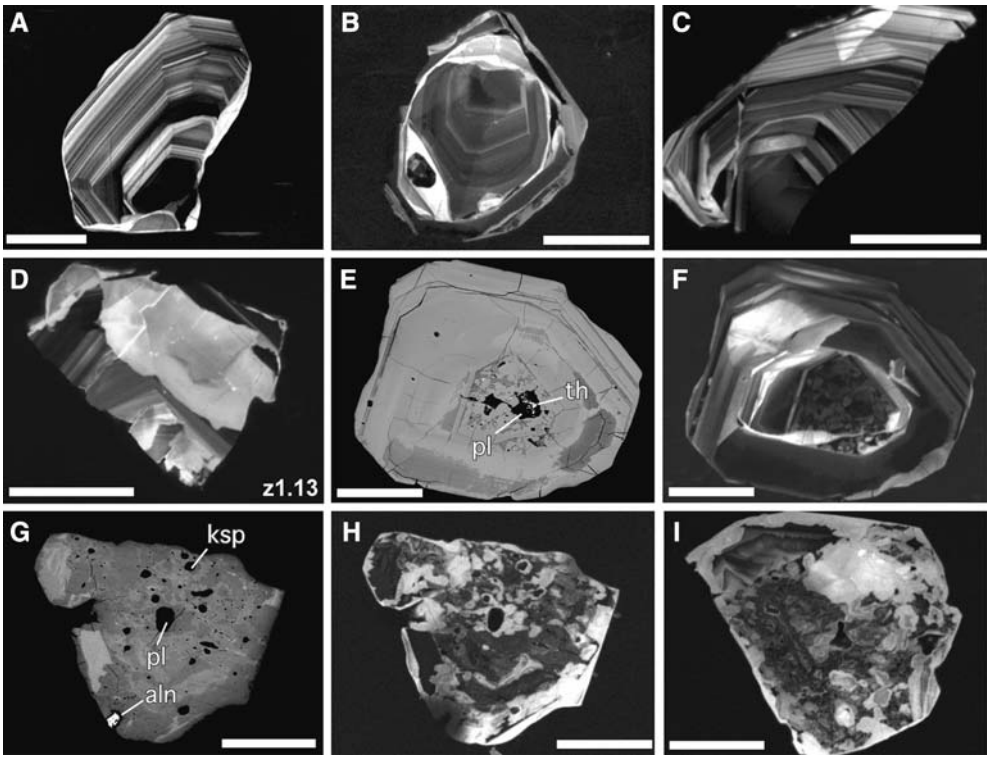

Fig. 3 BSE and CL images of type 1 (**e**–**i**) and type 2 (**a**–**c**) zircons from the McClure Mountain syenite. **e** and **g** are BSE images of the same zircons shown in CL in **f** and **h**, respectively. All other images are CL. *pl* plagioclase, *th* thorite, *aln* allanite, *ksp* K-feldspar. *Scale bars* are 100 μm. See text for discussion

whether or not this date represents crystallization of all or any of the baddeleyite is questionable.

Titanite and apatite

Nine titanite fractions were analyzed, including six single-grain fractions and three fractions with 2–3 grains each (Table 2). Grain diameter ranged from ~50 to 500 μm and grains were subhedral, bottle-brown to dark orange in color and free of visible inclusions. The seven apatite fractions each comprised between 4 and 7 sub- to euhedral grains that were clear, colorless, and free of inclusions and ranged from ~50 to 300 μm in diameter (Table 2). Two outliers in $^{207}Pb/^{206}Pb$–$^{238}U/^{206}Pb$ space (a4 and s6; determined to be outside 2 SD of the population; figure not shown) are plotted on concordia diagrams, but are excluded from weighted-mean dates and linear regressions. Age calculations from these data are sensitive to the choice of common Pb, due to the relatively low Pb^*/Pb_c ratios in both titanite (1.5–11) and apatite (1.3–2.1). The implications and methodology of deriving an adequate Pb_c correction is discussed below.

Feldspar

Single feldspar crystals ranging from 100 to 400 μm in diameter were hand-picked from non-magnetic separates and were free of inclusions or alteration. A random sample of ten of these grains was selected for EDS analysis and each was high-K feldspar. Five single-grain K-feldspar crystals were dissolved and analyzed by ID-TIMS for U–Pb isotopic composition (Table 2). These have low but variable U contents, and show significant scatter in isotope correlation diagrams (Fig. 6). One fraction of ~20 grains was subjected to a modified version of the step-wise leaching procedure of Housh and Bowring (1991) and analyzed for U–Pb isotopic compositions (Table 2; Fig. 6). The first two leaching steps were not analyzed and the fraction was completely dissolved by the sixth leaching step. The first analyzed leach step (Fsp2a) gives the least radiogenic Pb isotope composition ($^{206}Pb/^{204}Pb = 17.369 \pm 0.017$ and $^{207}Pb/^{204}Pb = 15.425 \pm 0.020$; Fig. 7), and is used as the closest approximation of initial Pb in feldspar for Pb_c corrections in titanite and apatite (as discussed below). The poor linear fit of these data on U–Pb isotope correlation diagrams (Fig. 6) indicates either that not all feldspar crystals had the same initial lead composition or that post-crystallization open-system behavior with respect to uranium and/or lead affected the grains.

Discussion

Inaccuracies due to U decay constants and ^{230}Th disequilibria

Several studies (Mattinson 1994, 2000; Schoene et al. 2006) have suggested that the mean values of one or both of the U decay constants may be inaccurate, as evidenced by normally discordant high-precision U/Pb

Table 1 U–Pb isotopic data for zircon and baddelleyite

Sample [a]	Pb^*/Pb_c [b]	Pb_c (pg) [c]	Th/U [d]	Isotopic ratios									Dates (Ma)						
				$^{206}Pb/^{204}Pb$ [e]	$^{208}Pb/^{206}Pb$ [f]	$^{206}Pb/^{238}U$ [f]	% err [g]	$^{207}Pb/^{235}U$ [f]	% err [g]	$^{207}Pb/^{206}Pb$ [f]	% err [g]	Corr. coef.	$^{206}Pb/^{238}U$ [h]	± [i]	$^{207}Pb/^{235}U$ [h]	± [i]	$^{207}Pb/^{206}Pb$ [h]	± [i]	% disc. [j]
Zircon																			
z1	49	1.40	0.88	2,707	0.277	0.084285	0.11	0.67209	0.15	0.05783	0.10	0.728	521.65	0.55	521.98	0.62	523.42	2.29	0.35
z2	31	1.87	0.89	1,756	0.278	0.084444	0.11	0.67378	0.16	0.05787	0.12	0.707	522.59	0.58	523.01	0.67	524.79	2.53	0.43
z3	26	1.24	0.56	1,589	0.175	0.084472	0.13	0.67444	0.19	0.05791	0.14	0.701	522.76	0.66	523.41	0.78	526.29	2.96	0.70
z12	29	0.98	0.74	1,676	0.231	0.084435	0.12	0.67339	0.20	0.05784	0.15	0.631	522.54	0.61	522.77	0.81	523.76	3.36	0.24
z13	34	1.03	0.81	1,952	0.255	0.084454	0.11	0.67330	0.16	0.05782	0.12	0.680	522.66	0.54	522.72	0.66	523.01	2.61	0.07
z14	29	2.57	0.75	1,666	0.240	0.083544	0.13	0.66695	0.18	0.05790	0.13	0.703	517.24	0.63	518.86	0.74	526.02	2.85	1.74
z1.13	29	2.20	1.05	1,559	0.331	0.084059	0.13	0.67131	0.19	0.05792	0.13	0.705	520.31	0.64	521.51	0.76	526.77	2.88	1.28
za1	508	1.18	21.39	4,874	6.609	0.084789	0.07	0.67478	0.11	0.05772	0.09	0.602	524.65	0.33	523.61	0.46	519.07	1.96	-1.12
za2	414	0.57	20.63	4,083	6.398	0.084752	0.08	0.67494	0.12	0.05776	0.08	0.699	524.43	0.41	523.71	0.48	520.62	1.84	-0.76
za3	1207	0.62	0.79	68,209	0.247	0.084671	0.07	0.67588	0.10	0.05789	0.07	0.702	523.94	0.36	524.28	0.42	525.74	1.59	0.36
za4	473	0.46	0.90	26,053	0.281	0.084665	0.05	0.67558	0.08	0.05787	0.06	0.671	523.91	0.26	524.10	0.32	524.92	1.28	0.20
za5	1987	0.43	1.53	95,093	0.481	0.084591	0.05	0.67524	0.07	0.05789	0.05	0.768	523.47	0.27	523.89	0.29	525.74	0.99	0.45
za6	547	0.44	15.50	6,774	4.878	0.084570	0.06	0.67554	0.09	0.05793	0.07	0.698	523.35	0.33	524.07	0.38	527.25	1.47	0.77
za7	3039	0.72	211.39	3,470	63.366	0.085356	0.08	0.67556	0.14	0.05740	0.12	0.587	528.02	0.41	524.09	0.59	507.03	2.58	-4.31
za8	92	1.68	1.25	4,701	0.391	0.084583	0.06	0.67503	0.10	0.05788	0.07	0.664	523.42	0.32	523.76	0.40	525.26	1.59	0.37
za9	539	0.26	13.54	7,459	4.248	0.084558	0.08	0.67491	0.12	0.05789	0.09	0.683	523.27	0.40	523.70	0.48	525.53	1.89	0.45
za10	746	0.29	0.75	42,552	0.235	0.084587	0.05	0.67580	0.07	0.05794	0.06	0.640	523.44	0.24	524.23	0.31	527.66	1.26	0.83
Baddelleyite																			
b1	28	2.59	0.55	1,672	0.167	0.086533	0.13	0.68915	0.20	0.05776	0.14	0.681	535.00	0.64	532.29	0.82	520.68	3.17	-2.87
b2	25	1.67	0.52	1,577	0.127	0.096993	0.19	0.75509	0.25	0.05646	0.15	0.801	596.76	1.10	571.17	1.07	470.56	3.26	-28.09
b3	103	1.44	0.06	6,792	0.019	0.084332	0.07	0.67300	0.10	0.05788	0.07	0.728	521.93	0.35	522.54	0.39	525.20	1.44	0.65
b4	48	17.22	0.01	3,269	0.004	0.084333	0.11	0.67299	0.15	0.05788	0.10	0.747	521.94	0.57	522.53	0.63	525.13	2.24	0.63
b5	22	3.18	0.10	1,466	0.033	0.084322	0.11	0.67209	0.14	0.05781	0.09	0.764	521.87	0.55	521.98	0.59	522.46	2.05	0.12
b7	121	1.31	0.09	7,965	0.029	0.084666	0.06	0.67577	0.09	0.05789	0.07	0.694	523.91	0.31	524.22	0.37	525.54	1.43	0.32
b8	14	1.13	1.58	747	0.501	0.084896	0.59	0.68056	0.64	0.05814	0.25	0.923	525.28	2.99	527.11	2.64	535.04	5.39	1.90
b9	34	1.71	0.56	2,069	0.159	0.088754	0.14	0.69858	0.17	0.05709	0.10	0.808	548.16	0.72	537.94	0.72	494.82	2.24	-11.25
b10	21	1.31	0.20	1,406	0.061	0.085515	0.26	0.67737	0.33	0.05745	0.19	0.810	528.96	1.34	525.18	1.36	508.80	4.28	-4.13
b11	31	2.19	0.28	2,012	0.089	0.083933	0.12	0.66862	0.15	0.05778	0.10	0.777	519.55	0.59	519.88	0.63	521.30	2.14	0.35
b12	6.8	5.36	0.07	494	0.021	0.084426	0.20	0.67298	0.27	0.05781	0.18	0.751	522.49	0.99	522.52	1.10	522.67	3.89	0.03
b13	2.4	5.70	0.22	186	0.066	0.084779	0.48	0.67137	0.97	0.05743	0.79	0.579	524.59	2.44	521.55	3.95	508.21	17.5	-3.36
b14	14	4.38	0.13	981	0.033	0.106350	0.12	0.84630	0.20	0.05771	0.15	0.659	651.51	0.77	622.61	0.92	518.91	3.27	-26.88
b15	4.7	1.01	1.52	328	0.414	0.104385	1.93	0.84719	2.10	0.05886	0.83	0.919	640.06	11.79	623.11	9.78	562.04	18.0	-14.58

[a] z1, z2, b1, b2, etc., are fractions composed of single grains. za1, za2, etc. are zircon fractions that were subjected to the chemical-abrasion technique. Zircon fractions in italics are group 1 zircons and those in plain text are group 2 zircons

[b] Ratio of radiogenic Pb (including 208Pb) to common Pb

[c] Total weight of common Pb

[d] Model Th/U ratio calculated from radiogenic 208Pb/206Pb ratio and 207Pb/206Pb age

[e] Measured ratio corrected for spike and fractionation only. Mass fractionation corrections were based on analysis of NBS-981 and NBS-983. Corrections of 0.25 ± 0.04%/amu (atomic mass unit) and 0.07 ± 0.04%/amu were applied to single-collector Daly analyses and dynamic Faraday–Daly analyses, respectively.

[f] Corrected for fractionation, spike and blank. All common Pb was assumed to be procedural blank

[g] Errors are 2 sigma, propagated using the algorithms of Ludwig (1980)

[h] Calculations are based on the decay constants of Jaffey et al. (1971)

[i] Errors are 2 sigma

[j] % discordance = 100–(100×206Pb/238U date/207Pb/206Pb date)

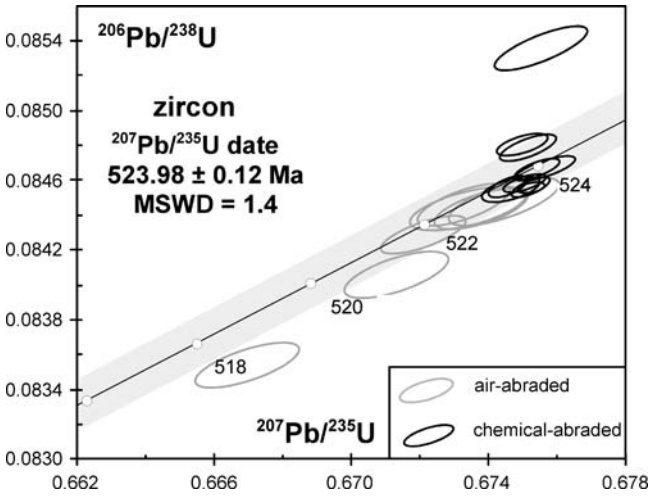

Fig. 4 Concordia diagram for zircon. Data are in Table 1. *Gray* band indicates error limits of the concordia curve. Calculated $^{207}Pb/^{235}U$ date includes all chemical-abraded grains. Errors are at the 95% confidence level

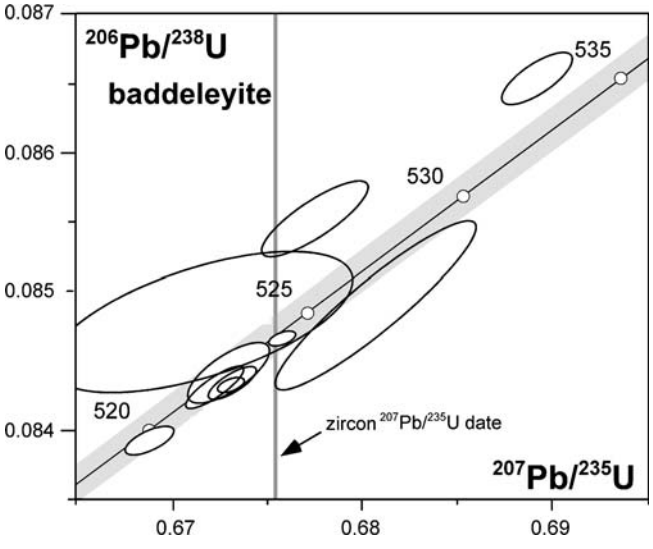

Fig. 5 Concordia diagram for baddeleyite. *Gray* band indicates the error limits of the concordia curve. Data are in Table 1. Errors are at the 95% confidence level

datasets spanning a wide range of time. Those studies imply that the real values of the decay constants are within the errors reported in the original alpha-counting experiments (Jaffey et al. 1971), but many authors note that the value of the ^{238}U decay constant is likely the more accurate of the two based on evaluation of the quality of the experiments (Begemann et al. 2001; Mattinson 1994, 2000; Schoene et al. 2006; Schön et al. 2004). Our zircon data are consistent with those conclusions, in that the chemical-abraded zircon analyses with Th/U of <20 are also slightly normally discordant. In this regard, it may be more accurate in an absolute sense to rely solely on the ^{238}U–^{206}Pb system for age calculations while using the $^{207}Pb/^{235}U$ date for evaluation of concordance/discordance only.

On the other hand, any mineral that has a Th/U ratio that differs from the magma or fluid from which it crystallized should be expected to have either an excess or deficiency in ^{206}Pb, which will affect the accuracy of the calculated $^{206}Pb/^{238}U$ date. While this phenomenon is most pronounced in monazite (Parrish 1990; Schärer 1984), it has previously been inferred to affect zircon systematics as well (Amelin and Zaitsev 2002; Oberli et al. 2004; Schmitz and Bowring 2001). Excess ^{206}Pb is a controlling factor in our zircon $^{206}Pb/^{238}U$ data, due in part to the variable abundance of high-Th mineral inclusions such as thorite and allanite, and possibly because of elevated Th levels in the zircon grains themselves. Correcting $^{206}Pb/^{238}U$ dates for excess ^{206}Pb requires either some knowledge of the Th/U of the melt from which the minerals crystallized (Parrish 1990; Schärer 1984) or by making the assumption that all minerals crystallized from a fluid with identical Th/U values, forcing data to converge upon a single $^{206}Pb/^{238}U$. Our data show that no single assumed value for the Th/U of the magma can cause the data to converge, proving that assumption to be incorrect in this case. The apatite and titanite populations are also likely affected by this problem, in that these minerals have model Th/U ratios of ~7–8 and 4–6 (Table 2), respectively, while that of the crystallizing magma is unconstrained. Several studies have also argued that excess ^{207}Pb in zircon, derived from non-equilibrium values of ^{231}Pa, can jeopardize $^{207}Pb/^{235}U$ dates (Amelin and Zaitsev 2002; Anczkiewicz et al. 2001; Mattinson 1973; Mortensen et al. 1992). However, these cases are relatively rare and the consistency of our $^{207}Pb/^{235}U$ dates from chemical-abraded zircons suggests that this is not an issue for the data reported in the present study.

Therefore, we choose to focus on the $^{207}Pb/^{235}U$ dates from zircon, titanite and apatite rather than the more precise $^{206}Pb/^{238}U$ dates. The trade-off in precision between the two methods is minimal compared to the potential inaccuracies introduced by excess ^{206}Pb. Any inaccuracy in the ^{235}U decay constant will introduce a systematic error, but will not affect the relative offset between the closure dates of the different minerals (for example, the data in Schoene et al. (2006) would predict an offset of 0.1% between $^{206}Pb/^{238}U$ and $^{207}Pb/^{235}U$ dates). Therefore, the cooling history of the rock and any potential bias with the $^{40}Ar/^{39}Ar$ method may still be addressed accurately. If future work results in refinement of the ^{235}U decay constant, correcting these dates to be more accurate in absolute time is a trivial issue.

Common Pb correction

The apatite and titanite dates are heavily dependent on the correction used for the initial isotopic composition of lead (a.k.a. common lead; Pb_c), which can be chosen using several methods: (1) selecting a composition based on a bulk Pb evolution model, such as that in Stacey and

Table 2 U–Pb isotopic data for titanite, apatite and K-feldspar

Sample[a]	No. of grains[b]	Pb*/ Pb_c[c]	Pb_c[d] (pg)	Th/ U[e]	Isotopic ratios							Corr. coef.		
					$^{208}Pb/^{206}Pb$[f]	$^{238}U/^{206}Pb$[f]	% err[g]	$^{207}Pb/^{206}Pb$[f]	% err[g]	$^{204}Pb/^{206}Pb$[f]	% err[g]	238/206–207/206	238/206–204/206	207/206–204/206
Titanite														
t1	1	4.4	34.3	4.9	1.55	10.38763	0.16	0.15790	0.62	0.00689	0.98	−0.21	0.00	−0.44
t3	3	6.3	46.7	5.0	1.58	10.74977	0.10	0.13262	0.41	0.00515	0.74	−0.25	0.00	−0.59
t5	4	5.8	28.2	5.2	1.62	10.64344	0.15	0.13862	0.71	0.00555	1.23	−0.19	0.00	−0.35
t6*	3	4.1	54.5	5.0	1.61	10.20520	0.12	0.16816	0.39	0.00758	0.60	−0.32	0.00	−0.63
t7	2	4.8	32.1	5.6	1.73	10.40264	0.17	0.15698	0.66	0.00682	1.05	−0.20	0.00	−0.41
t8	1	1.5	19.6	4.2	1.30	8.74440	0.58	0.26999	1.16	0.01461	1.52	−0.26	0.00	−0.16
t9	1	11.2	8.2	5.9	1.79	11.22827	0.29	0.09914	2.14	0.00284	5.15	−0.04	0.00	−0.17
t10	1	4.2	10.3	4.2	1.31	10.56132	0.47	0.14577	2.21	0.00605	3.71	−0.13	0.00	−0.11
t11	1	6.4	6.9	4.6	1.34	10.99103	0.51	0.11642	3.13	0.00402	6.26	−0.04	0.00	−0.22
Apatite														
a1	4	2.1	184.0	8.1	2.35	8.33778	0.15	0.29907	0.12	0.01669	0.17	−0.34	0.00	−0.746
a2	7	1.8	374.3	7.0	2.20	8.16325	0.16	0.31300	0.07	0.01763	0.12	-0.37	0.00	-0.785
a3	4	1.3	309.4	7.0	2.08	7.47699	0.21	0.36058	0.07	0.02097	0.15	−0.43	0.00	−0.591
a4*	7	1.3	83.3	7.2	2.22	7.11610	0.28	0.38104	0.23	0.02229	0.28	−0.30	0.00	−0.716
a5	5	1.7	242.8	8.2	2.36	7.80379	0.18	0.33653	0.09	0.01929	0.14	−0.36	0.00	−0.794
a6	4	1.9	524.4	8.1	2.37	8.07804	0.15	0.31969	0.06	0.01812	0.10	−0.37	0.00	−0.885
a7	7	1.4	188.6	8.0	2.26	7.21837	0.22	0.37785	0.11	0.02215	0.15	−0.37	0.00	−0.744
K-feldspar														
Total dissolution														
F1	1	0.07	293.4	NA	2.04	0.00968	2.51	0.88715	0.04	0.05753	0.10	−0.66	0.00	−0.730
F2	1	0.07	187.2	NA	1.98	0.03749	2.34	0.88467	0.04	0.05708	0.09	−0.61	0.00	−0.861
F3	1	0.07	708.7	NA	2.08	0.00016	2.45	0.88780	0.04	0.05747	0.09	−0.65	0.00	−0.897
F4	1	0.31	141.6	NA	1.99	0.00892	0.74	0.88781	0.05	0.05734	0.13	0.11	0.00	−0.515
F5	1	0.31	184.0	NA	2.02	0.00213	0.66	0.88808	0.05	0.05731	0.13	0.12	0.00	−0.512
Step-leaching														
Fsp2.a	~20	0.00	10675.8	NA	2.12	0.00396	1.50	0.88806	0.04	0.05757	0.10	−0.90	0.00	−0.819
Fsp2.b	~20	0.31	439.4	NA	2.07	0.00916	0.55	0.88815	0.04	0.05752	0.11	0.22	0.00	−0.706
Fsp2.c	~20	0.31	353.5	NA	2.05	0.01724	0.55	0.88791	0.05	0.05749	0.10	0.24	0.00	−0.697
Fsp2.d	~20	0.31	113.8	NA	2.01	0.00813	0.76	0.88744	0.19	0.05738	0.09	0.09	0.00	−0.200

[a] t1, a1, F1 refer to mineral fraction analyzed. Fsp2.a, .b, .c, .d refer to sequential leaching step

[b] Number of grains dissolved in fraction. For step-leaching, a total of ~20 grains were used and progressively leached

[c] Ratio of radiogenic Pb (including 208Pb) to common Pb

[d] Total weight of common Pb

[e] Model Th/U ratio calculated from radiogenic 208Pb/206Pb ratio, reduced using the common Pb values determined by the total Pb–U isochron. *NA* not applicable, because feldspar are not radiogenic enough to perform that calculation

[f] Measured ratio corrected for spike, fractionation, and blank only. Mass fractionation corrections were based on analysis of NBS-981 and NBS-983. Corrections of 0.25 ± 0.04%/amu (atomic mass unit) and 0.07 ± 0.04%/amu were applied to single-collector Daly analyses and dynamic Faraday–Daly analyses, respectively. A Pb blank of 1.5 ± 0.4 pg and a U blank of 0.10 ± 0.05 pg were applied to all data

[g] Errors are 2 sigma, propagated using the algorithms of Ludwig (1980)

*Fractions that were not used in regressions or weighted-means

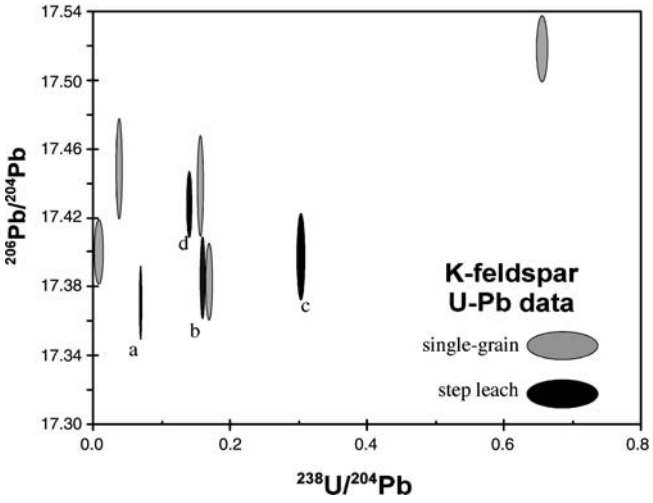

Fig. 6 U–Pb isotope correlation diagram for K-feldspar. Data are in Table 2. See text for discussion. Errors are at the 95% confidence level

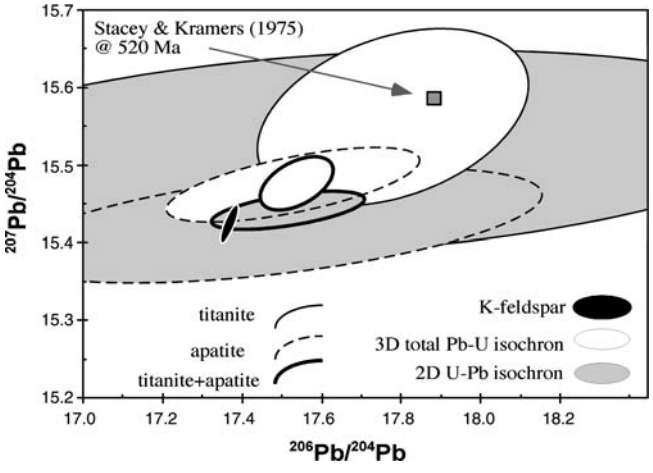

Fig. 7 Pb isotope correlation diagram depicting the Pb_c values derived by different methods for correcting U–Pb titanite and apatite data. See text for discussion. Errors are at the 95% confidence level

Kramers (1975); (2) determining and applying the Pb isotopic composition of cogenetic low-U minerals; or (3) employing 2-D and 3-D isochron regression techniques, in which the intercept of a line with one of the axes describes the best-fit Pb_c composition. Several studies have investigated the effects of using a Pb_c correction derived from the Stacey and Kramers (1975) two-stage Pb-evolution model in comparison to those extracted from coexisting low-U minerals such as K-feldspar (e.g., Chamberlain and Bowring 2000; Corfu 1988; Mezger and Cosca 1999; Schmitz and Bowring 2001; Verts et al. 1996). The latter methods are deemed to yield more accurate dates because, in general, the data are sensitive enough to the choice of Pb_c that it is difficult to justify an ad hoc correction using a model Pb_c composition; in some cases the U–Pb dates reduced with feldspar Pb also plot closer to concordia. However, Chamberlain and Bowring (2000) note that in one sample, a poor linear fit of apatite and feldspar in $^{207}Pb/^{204}Pb$–$^{206}Pb/^{204}Pb$ space suggests that the two minerals do not meet one of the required assumptions: that the minerals were in isotopic equilibrium at a mutual time of crystallization and that each phase has remained closed with respect to U and Pb since that time. We attempt here to test those assumptions further by measuring U–Pb systematics of K-feldspar and using 2-D U–Pb isochrons or the 3-D total Pb-U isochron (Ludwig 1998) to constrain whether those assumptions are met.

We have calculated the $^{206}Pb/^{204}Pb$ and $^{207}Pb/^{204}Pb$ values for Pb_c in titanite and apatite using each of the techniques described above. The results are shown in Fig. 7 and the data reduced with those compositions are plotted in concordia space in Fig. 8. It is easy to distinguish the K-feldspar Pb isotopic values from the Stacey and Kramers (1975) values at 520 Ma (Fig. 7). The calculated $^{206}Pb/^{204}Pb$ and $^{207}Pb/^{204}Pb$ values from the 2-D isochron regressions overlap with the feldspar data, though the apatite data are discernibly less radiogenic than the Stacey and Kramers (1975) estimate and the calculated initials are relatively imprecise. The least radiogenic feldspar datum (corresponding to the first leach step which contained minimal U; Fsp2a) lies outside the Pb_c compositions calculated from the 3-D total Pb–U isochron regressions of titanite and apatite (Fig. 7). The added precision of regressing titanite and apatite together on the 3-D isochron yields a result with higher precision than with each phase individually, but gives an unacceptably high MSWD of linearity (~3–10; isochrons are not shown). This is also true for regressions involving apatite, titanite and K-feldspar (MSWDs are ~3–10), suggesting these minerals were not in isotopic equilibrium at any moment in time or that open-system behavior was important.

It should be noted that the 3-D total Pb-U isochron utilizes both U decay schemes, and therefore the result may be affected by ^{230}Th disequilibrium. As a sensitivity test, the ratios uncorrected for non-blank Pb_c (Table 1) were corrected for excess ^{206}Pb using methods similar to those in Schärer (1984) and Parrish (1990) for various magmatic Th/U ratios. This test shows that while the calculated dates can vary significantly (e.g., can lower apatite dates by 1–2 Myr for Th/U of the magma between 5 and 1), the calculated initial Pb isotopic compositions are insensitive. Therefore, for all dates calculated using isochron Pb_c estimates, the Pb_c compositions and the associated errors are used to reduce the raw U–Pb data and the resulting $^{206}Pb/^{238}U$ and $^{207}Pb/^{235}U$ ratios are plotted in concordia space and used to calculate weighted-mean dates (Fig. 8; the resulting dates are summarized in Fig. 9).

A further caveat lies in that titanite fractions have less total Pb than either apatite or feldspar, and are therefore potentially more sensitive to the effect of Pb blank on the resulting 3-D isochron solution. A sensitivity test shows that using blank values of 0–10 pg has a negligible effect on the calculated initial $^{207}Pb/^{204}Pb$, but using

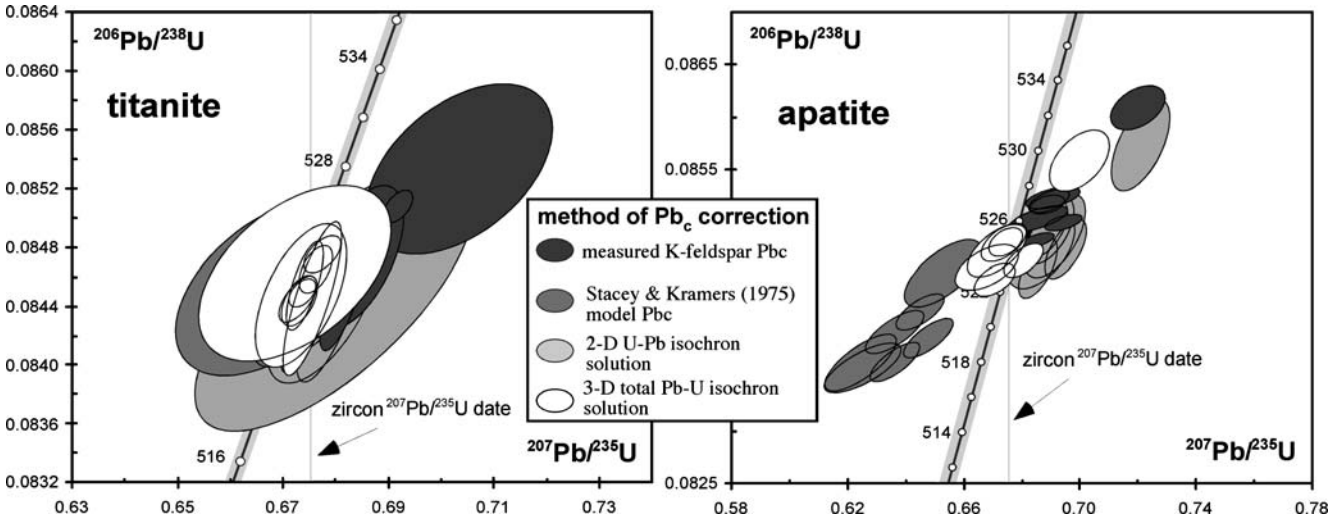

Fig. 8 Concordia diagrams for titanite and apatite depicting the effect of different Pb_c corrections on the data. See text for discussion. Uncorrected data are in Table 2, and a summary of the weighted-mean $^{207}Pb/^{235}U$ dates, errors, and MSWDs are in Fig. 9. *Gray* band indicates error limits of the concordia curve. Errors are at the 95% confidence level

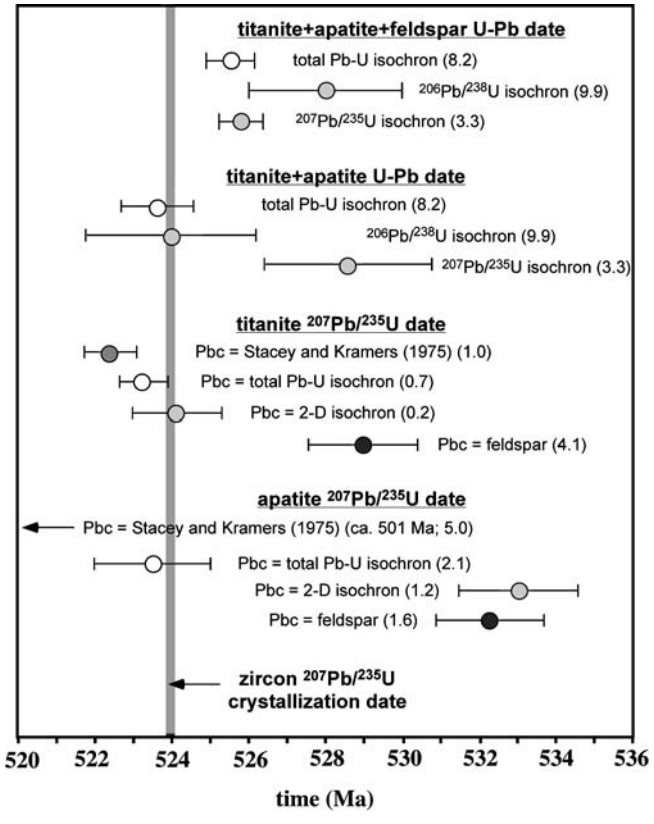

Fig. 9 Summary diagram for the Pb_c correction in titanite and apatite. *Numbers* in *parentheses* indicate the MSWD of the linear regressions (for multi-phase U–Pb dates) or weighted-mean dates (single phase $^{207}Pb/^{235}U$ dates—method of calculation described in text). Values of Pb_c are depicted in Fig. 7 and concordia diagrams with each Pb_c composition are in Fig. 8. Errors are at the 95% confidence level

blank values of >5 pg has considerable affect on the calculated initial $^{206}Pb/^{204}Pb$ and on the U–Pb date calculated with the 3-D regression (for example, a 5 pg blank returns a U–Pb date of 523.2 ± 3.9 Ma and an initial $^{206}Pb/^{204}Pb$ of 17.7 ± 1.4 and $^{207}Pb/^{204}Pb$ of 15.5 ± 0.4 with an MSWD $= 0.1$ and a 10 pg blank returns a U–Pb date of 532.9 ± 3.7 Ma and an initial $^{206}Pb/^{204}Pb$ of 13.9 ± 3.6 and $^{207}Pb/^{204}Pb$ of 15.5 ± 3.5 with an MSWD $= 9.4$). However, a Pb blank of >5 pg is unreasonable for these data because of the consistency of total procedural blanks (which fall between 1 and 2 pg), the fact that low-Pb single grain fractions have ≤ 10 pg total Pb_c, and an increasingly poor linear fit of the data and correspondingly large errors of the resulting Pb_c values. Therefore, we consider the Pb blank of 1.5 ± 0.4 pg to be robust, and the resulting initial Pb_c values and U–Pb dates to be accurate.

Picking the best Pb_c composition is easily done in concordia space (Fig. 8) if we assume that the titanite and apatite data are most likely within error of concordia or normally discordant and that the cooling dates must be less than or equal to the zircon crystallization age. The apatite dataset is especially sensitive to the choice of Pb_c because these data overall have lower and more variable Pb^*/Pb_c. These data show substantial scatter and are negatively discordant when using the Stacey and Kramers (1975) Pb_c correction, and the amount of offset from concordia correlates roughly with the Pb^*/Pb_c of the individual analyses. Using the less radiogenic estimates shifts the data closer to concordia, though both the 2-D isochron solution and the feldspar Pb_c values shift the data to values that are normally discordant and older than the zircon date. The titanite data are less sensitive to the choice of Pb_c composition, though feldspar-corrected data also fall normally discordant with a weighted-mean $^{207}Pb/^{235}U$ date that is substantially older than with other Pb_c estimates (Fig. 9). The total Pb–U isochron solutions for titanite and apatite yield concordant results with weighted-mean $^{207}Pb/^{235}U$ dates that overlap with the zircon $^{207}Pb/^{235}U$ date (Figs. 8, 9).

We conclude that the best composition of Pb_c for both titanite and apatite are the values determined by the total Pb–U isochron, and that these values are different from one another (Figs. 7, 8, 9; best-fit compositions are as follows: titanite $^{206}Pb/^{204}Pb = 17.79 \pm 0.34$, $^{207}Pb/^{204}Pb = 15.56 \pm 0.10$; apatite $^{206}Pb/^{204}Pb = 17.54 \pm 0.27$, $^{207}Pb/^{204}Pb = 15.47 \pm 0.04$). Additionally, neither thermochronometer is amenable to the feldspar Pb_c and therefore all three phases have different average Pb_c compositions. The best estimate weighted-mean $^{207}Pb/^{235}U$ closure dates for titanite and apatite are $523.26 \pm 0.65/0.72/1.27$ Ma (MSWD = 0.7) and $523.51 \pm 1.47/1.53/2.09$ Ma (MSWD = 2.1; internal errors/with tracer calibration errors/with tracer calibration and decay constant errors), respectively (Fig. 9).

Thermal and petrologic history of the rock

Given that the best estimates for Pb_c differ for titanite, apatite and K-feldspar, we must conclude that the minerals were not in isotopic equilibrium at the time of their respective crystallization or that subsequent open-system behavior affected the U–Pb systematics. There are several end-member explanations for the observed variations in Pb isotope systematics: (1) that the minerals incorporated Pb with variable isotopic compositions at the time of crystallization; (2) that the isotopic signatures changed as a function of time during cooling due to interaction with reservoirs of variable Pb_c composition; or (3) that mineral alteration and recent weathering compromised closed-system behavior. Option 3 is unlikely both because of the freshness of the rock and the minerals analyzed and because such processes would also substantially disturb the age information recorded in titanite and apatite, which is not observed. If the first option is true, it requires that on average, the three phases crystallized from reservoirs of Pb with distinct isotopic signatures. Given that petrographically, titanite, apatite and feldspar likely have significant overlap in the timing of crystallization and are often in contact with one another, this option seems unlikely to be entirely responsible for the observed variation. In addition, this option would require that the minerals were able to retain a distinct isotopic signature above their respective closure temperatures in an environment that had magmas/fluids with fluctuating or evolving Pb isotopic values.

The best explanation for the observed differences in initial Pb_c composition in titanite, apatite and K-feldspar is that the average isotopic composition of the lead incorporated in each mineral is a function of differing closure temperatures and therefore reflects a changing composition of lead in the system during cooling. Mineralogical and textural features in our sample show that the composition of the magma and associated fluids changed with respect to major and trace element chemistry as a function of space (e.g., within the scale of a thin-section) and/or time. This is evidenced by the presence of calcite, baddeleyite and nepheline, which are not distributed homogeneously throughout the rock, but instead occur together in discrete millimeter-sized zones (Figs. 1b, 2c). K-feldspar and plagioclase symplectite texture (Fig. 1b) also occur in these zones, and this texture is often interpreted to reflect subsolidus quenching perhaps following the removal of a fluid-rich component (Fenn 1986; Lofgren 1980). Therefore, we infer that intercumulus or late-stage fluid became CO_2-rich and Si-undersaturated late in the rock's crystallization history. It seems reasonable then that the Pb isotopic composition of the fluids may have changed with time and/or space as well; therefore, minerals with different closure temperatures would retain different isotopic compositions of Pb_c at their time of closure to diffusion. Evidence consistent with this interpretation comes from Armbrustmacher and Hedge (1982), who conducted a trace element and Sr-isotope study of the McClure Mountain complex and showed that the main body of the nepheline syenite, which post-dates the hornblende–biotite syenite, has distinctly less-radiogenic Sr isotopic values. They concluded that this is indicative of multiple distinct source regions for the different magmatic compositions of the complex. We should note also that the U–Pb data from baddeleyite are consistent with this model. Though the potential for open-system behavior in these data complicates their interpretation, the weighted-mean $^{207}Pb/^{235}U$ date of four equivalent points (Fig. 5) is ~1–1.5 Ma younger than the zircon date; if this date is robust, it is consistent with their crystallization being concurrent with a late-stage fluid evolving towards Si-undersaturation.

Whether or not titanite, apatite and K-feldspar could equilibrate with the Pb isotopic characteristics of a host fluid during cooling is dependent on the balance between the rates of fluid advection through the rock and volume diffusion of Pb within individual minerals. Typical values for nominal closure temperatures for diffusion of Pb in titanite and apatite (T_c = ~600–650°C and ~450–550°C, respectively) are derived from a combination of diffusion experiments (Cherniak 1993; Cherniak et al. 1991), crystal-chemical theory based on ionic porosity (Dahl 1997), and the consistency of numerous geologic studies (e.g., Chamberlain and Bowring 2000; Corfu 1988; Corfu and Stone 1998; Mezger et al. 1991; Nemchin and Pidgeon 1999). A simple calculation using the diffusion parameters for apatite from Cherniak et al. (1991) shows that if the rock remained at a constant temperature of 575°C for 1–2 Myr (the maximum offset in closure dates between apatite and titanite), one would expect diffusion of Pb to be important in apatite on length-scales of 100–150 μm. Given that the radii of apatite cylinders analyzed in this study vary between 50 and 150 μm, and that the rates of grain boundary diffusion are far greater than volume diffusion (e.g., Joesten 1992), it is reasonable that apatite could equilibrate with a fluid that is temporally variable with respect to the Pb isotopic composition over those timescales.

The closure temperature of Pb in K-feldspar is not well constrained, though the diffusion experiments of

Cherniak (1995) suggest that under anhydrous conditions Pb is less mobile than in apatite. Because feldspar lacks sufficient U to be a good U–Pb thermochronometer, there are no field-based tests to verify the diffusion experiments and the effect of hydrous conditions are unknown but potentially important. If the closure temperature of feldspar with respect to Pb is higher than apatite, then the evolution of the Pb isotopic values of the interacting fluid would have to fluctuate up and down as a function of time because the feldspar Pb_c estimates are less radiogenic than the apatite total Pb–U isochron estimate (Fig. 7). If the closure temperature for Pb in K-feldspar is in fact lower than apatite (Chamberlain and Bowring 2000), a simpler single-stage model is more appropriate where the isotopic composition of Pb in the fluid evolves towards less radiogenic values with time. The excess scatter in U–Pb data from titanite, apatite and feldspar, evidenced by high MSWDs and outliers in isotope correlation diagrams (e.g., Figs. 6, 9) may be suggestive of more complicated interaction of mineral growth, volume and grain boundary diffusion of Pb, and transport of Pb of different compositions by magmatic fluids during cooling. It may also be a reflection of the grain-size dependency on closure temperature (Dodson 1973, 1986), partial equilibration of Pb_c composition, or armoring of mineral-inclusions that prevents fluid–mineral interaction entirely (Loferski and Ayuso 1995; Meurer and Boudreau 1996; Willmore et al. 2000).

The implications of our observations of variable Pb_c compositions in different phases in the rock go beyond a petrologic model and are applicable more generally to U–Pb thermochronology. The accuracy of some studies relies on correctly assigning a Pb_c composition to the data and in slowly cooled rocks, typical of Archean and Proterozoic terranes, the methods used here may not be applicable. The grain-size dependence on closure temperature of thermochronometers means that neither 2-D nor 3-D isochrons are valid methods of Pb_c composition determination in slowly cooled rocks. Making a correction with the isotopic composition of cogenetic low-U minerals such as K-feldspar may also be inaccurate. The importance of this point to a given study is of course dependent on the sensitivity of an interpretation to a Pb_c correction. For example, in minerals that are periodically or permanently open to diffusion for hundreds of millions or billions of years (e.g., Schmitz and Bowring 2003), there is a far greater time period in which different fluids may act as reservoirs for Pb_c, but any inaccuracy introduced with that correction may be unimportant compared to the magnitude of the spread in U–Pb dates. For studies that pursue relatively short-duration, high-precision cooling histories or intermethod comparison, the Pb_c correction is of utmost importance.

Intercalibration of U–Pb and $^{40}Ar/^{39}Ar$ from MMhb

Because K–Ar and $^{40}Ar/^{39}Ar$ hornblende dates from MMhb are cooling dates, we have established a context within the U–Pb system to which dates can be compared. Given the high-precision, relatively fast, cooling path constrained by the ^{235}U–^{207}Pb system, and that the closure temperature of Ar in hornblende is between titanite and apatite ($T_c = 500$–$550°C$; McDougall and Harrison 1999), the $^{40}Ar/^{39}Ar$ cooling date should fall, within internal errors, between the lower-bound $^{207}Pb/^{235}U$ date of apatite and the upper-bound $^{207}Pb/^{235}U$ date of titanite, or 522.98 ± 1.00 Ma (including tracer calibration errors, but not decay constant errors) if no bias existed between the two systems (Fig. 10).

MMhb ranks among the most-dated minerals by the K–Ar and $^{40}Ar/^{39}Ar$ methods, despite the fact that its homogeneity and quality as a standard are often questioned. Baksi et al. (1996) showed that unpurified 15 mg splits of MMhb show isotopic inhomogeneity, giving $^{40}Ar/^{39}Ar$ dates ranging from 513.5 ± 1.4 to 520.4 ± 1.8 Ma with respect to the SB–3 biotite at 162.9 Ma, and concluded that MMhb is unsuitable as a fluence monitor in $^{40}Ar/^{39}Ar$ geochronology. This concern is supported by previous work summarized in Baksi et al. (1996) and also in subsequent intercalibration studies by Renne et al. (1998b) and Spell and McDougall (2003), who find inhomogeneity in total-fusion analyses relative to the Fish Canyon sanidine and GA-1550 biotite. Inhomogeneity in dates for MMhb is likely derived from impure separates or inclusions of high-K minerals such as biotite and K-feldspar (Lee et al. 1991; Villa et al. 1996). Incremental heating experiments on MMhb support this inference in that early heating steps show anomalously low apparent ages, though resulting plateau dates yield highly consistent results (Lee et al. 1991; Rex et al. 1993; Villa et al. 1996). Despite evidence for inhomogeneity in MMhb, continued work to recollect and proliferate this standard is being carried out (Kunk et al. 1994; Kunk and Miller 2002), emphasizing the importance of attaining an accurate reference date and further characterizing under what conditions this standard can be considered homogeneous.

The most widely cited reference dates for MMhb are the K–Ar compilation date from Samson and Alexander (1987) of 520.4 ± 3.4 Ma and the total-fusion $^{40}Ar/^{39}Ar$ dates from Renne et al. (1998b) of 523.1 ± 5.2 and from Spell and McDougall (2003) of 523.3 ± 1.8 Ma, referenced to the primary biotite standard GA-1550 using K–Ar ages of 98.8 ± 1.9 and 98.5 ± 1.6, respectively ($^{40}Ar/^{39}Ar$ dates include intercalibration errors, but not decay constant errors). These K–Ar and $^{40}Ar/^{39}Ar$ dates return apparent biases of 0.5 ± 0.7, 0.0 ± 1.0, and $0.0 \pm 0.4\%$ with respect to the ^{235}U–^{207}Pb system (excluding decay constant errors; Fig. 10). A robust $^{206}Pb/^{238}U$ date would likely be younger than the $^{207}Pb/^{235}U$ date by ~0.1% (ca. 0.5 Myr) given tangible inaccuracies in the U decay constants (Mattinson 2000; Schoene et al. 2006). Though each date overlaps within internal error of the predicted $^{207}Pb/^{235}U$ date, the K–Ar date has a high probability of being different than the $^{207}Pb/^{235}U$ date. The offsets between the U–Pb and

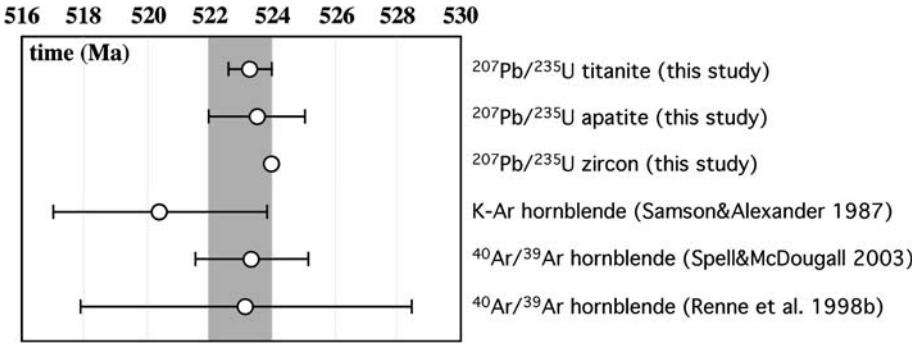

Fig. 10 Summary comparing popular K–Ar and $^{40}Ar/^{39}Ar$ dates from the literature with $^{207}Pb/^{235}U$ dates from this study. *Gray* band marks the expected closure time of hornblende based on the maximum and minimum closure times of titanite and apatite, respectively. *Errors* on U–Pb dates include tracer calibration errors but not decay constant errors. *Error bars* for zircon date are smaller than the *symbol*. Errors on $^{40}Ar/^{39}Ar$ dates include intercalibration errors but not errors for the primary standard used or for the decay constants or physical constants of ^{40}K. All errors are at the 95% confidence level

$^{40}Ar/^{39}Ar$ dates are consistent with previous observations that U–Pb dates are often systematically older than $^{40}Ar/^{39}Ar$ dates by $\leq 1.0\%$ (Min et al. 2000, 2001; Renne 2000; Renne et al. 1998a; Schoene et al. 2006) if only internal errors are considered. However, these data are also consistent with there being no bias between the two methods. Assessing more precisely any bias with respect to MMhb would be aided by higher-precision $^{40}Ar/^{39}Ar$ dates. This goal may be realized through the intercalibration of MMhb against other $^{40}Ar/^{39}Ar$ standards using purified separates and the step-heating method both because of the potential for greater precision and the added benefit of evaluating concordancy. Such a study—in combination with our U–Pb age—may further reveal whether MMhb is a suitable standard for geochronology or whether it should be abandoned for a more suitable reference material.

Conclusions

The McClure Mountain syenite yields two populations of zircon, and the abundance of high-Th inclusions in one population and sporadically high-Th contents in the other negate the use of the $^{206}Pb/^{238}U$ date. A weighted mean $^{207}Pb/^{235}U$ date from ten chemical-abraded zircon fractions of $523.98 \pm 0.12/0.18/0.74$ Ma (MSWD = 1.4; internal errors/with tracer calibration errors/with tracer calibration and decay constant errors) is our best estimate for the crystallization age of the syenite.

We explore the best correction for the isotopic composition of initial Pb (Pb_c) in titanite and apatite and K-feldspar, and show that the composition is different for each mineral. This implies that using a single Pb_c correction for multiple U–Pb thermochronometers may be inaccurate, especially in rocks that have complicated late-stage magmatic or hydrothermal histories or in slowly cooled rocks.

A possible model to explain this involves a late-stage magmatic fluid, whose Pb isotopic composition changed as a function of time, controlled the composition of Pb_c in each mineral phase at the time of its respective closure to diffusion of Pb.

The $^{207}Pb/^{235}U$ cooling dates for titanite and apatite are $523.26 \pm 0.65/0.72/1.27$ Ma (MSWD = 0.7) and $523.51 \pm 1.47/1.53/2.09$ Ma (MSWD = 2.1; internal errors/with tracer calibration errors/with tracer calibration and decay constant errors), respectively.

U–Pb thermochronologic data yield a best estimate closure date for Ar in hornblende of 522.98 ± 1.00 Ma with respect to the ^{235}U–^{207}Pb system, from which intermethod biases may be assessed. While these data are consistent with previous studies that show K–Ar and $^{40}Ar/^{39}Ar$ dates to be younger than U–Pb dates by $\leq 1\%$, they are also consistent with there being no bias. The ambiguity is primarily a result of large errors in the K–Ar and $^{40}Ar/^{39}Ar$ dates, which may be a result of the inhomogeneity in MMhb pointed out by other workers.

Acknowledgments Helpful reviews by J. Hanchar and an anonymous reviewer made this an overall better paper. This work was supported in part by NSF grant EAR 0451802 (The EARTHTIME Network: Developing an infrastructure for high-resolution calibration of Earth History) to S. Bowring. Additional support was provided to B. Schoene by a subaward from NSF grant EAR 031521 (CHRONOS to C. Cervato).

References

Alexander JEC, Mickelson GM, Lanphere MA (1978) MMhb-1: a new ^{40}Ar-^{39}Ar dating standard. In: Zartman RE (ed) Short papers of the fourth international conference, geochronology, cosmochronology, and isotope geology, vol 78–701. US Geological Survey, Open-File report, pp 6–8

Amelin Y, Zaitsev AN (2002) Precise geochronology of phoscorites and carbonatites: the critical role of U-series disequilibrium in age interpretations. Geochim Cosmochim Acta 66(13):2399–2419

Anczkiewicz R, Oberli F, Burg JP, Villa IM, Gunther D, Meier M (2001) Timing of normal faulting along the Indus Suture in Pakistan Himalaya and a case of major $^{231}Pa/^{235}U$ initial disquilibrium in zircon. Earth Planet Sci Lett 191:101–114

Armbrustmacher TJ, Hedge CE (1982) Genetic implications of minor-element and Sr-isotope geochemistry of alkaline rock complexes in the Wet Mountains area, Fremont and Custer counties, Colorado. Contrib Miner Petrol 79:424–435

Baksi AK, Archibald DA, Farrar E (1996) Intercalibration of $^{40}Ar/^{39}Ar$ dating standards. Chem Geol 129:307–324

Begemann F, Ludwig KR, Lugmair GW, Min K, Nyquist LE, Patchett PJ, Renne PR, Shih C-Y, Villa IM, Walker RJ (2001) Call for an improved set of decay constants for geochronological use. Geochim Cosmochim Acta 65(1):111–121

Chamberlain KR, Bowring SA (2000) Apatite–feldspar U–Pb thermochronometer: a reliable mid-range (~450C), diffusion controlled system. Chem Geol 172:173–200

Cherniak DJ (1993) Lead diffusion in titanite and preliminary results on the effects of radiation damage on Pb transport. Chem Geol 110:177–194

Cherniak DJ (1995) diffusion of Pb in plagioclase and K-feldspar investigated using Rutherford backscatter and resonant nuclear reaction analysis. Contrib Miner Petrol 120:358–371

Cherniak DJ, Watson EB (2000) Pb diffusion in rutile. Contrib Miner Petrol 139:198–207

Cherniak DJ, Lanford WA, Ryerson FJ (1991) Lead diffusion in apatite and zircon using ion implantation and Rutherford Backscattering techniques. Geochim Cosmochim Acta 55:1663–1673

Corfu F (1988) Differential response of U–Pb systems in coexisting accessory minerals, Winnepeg River Subprovince, Canadian Shield: implications for Archean crustal growth and stabilization. Contrib Mineral Petrol 98:312–325

Corfu F, Stone D (1998) The significance of titanite and apatite U–Pb ages: Constraints for the post-magmatic thermal–hydrothermal evolution of a batholithic complex, Berens River area, northwestern Superior Province, Canada. Geochim Cosmochim Acta 62(17):2979–2995

Corfu F, Hanchar JM, Hoskin PWO, Kinny P (2003) Atlas of zircon textures. In: Hanchar JM, Hoskin PWO (eds) Zircon, vol 53. Mineralogical Society of America, Washington, D.C., pp 468–500

Dahl PS (1997) A crystal-chemical basis for Pb retention and fission-track annealing systematics in U-bearing minerals, with implications for geochronology. Earth Planet Sci Lett 150:277–290

Dodson MH (1973) Closure temperature in cooling geochronological and petrological systems. Contrib Mineral Petrol 40:259–274

Dodson MH (1986) Closure profiles in cooling systems. Mater Sci Forum 7:145–154

Fenn PM (1986) On the origin of graphic granite. Amer Min 71:325–330

Frost BR, Chamberlain KR, Schumacher JC (2000) Sphene (titanite): phase relations and role as a geochronometer. Chem Geol 172:131–148

Gerstenberger H, Haase G (1997) A highly effective emitter substance for mass spectrometric Pb isotope ratio determinations. Chem Geol 136:309–312

Grove M, Harrison TM (1996) $^{40}Ar^*$ diffusion in Fe-rich biotite. Amer Mineral 81:940–951

Hanchar JM, Hoskin PWO (2003) Reviews in mineralogy and geochemistry: zircon, vol 53. The Mineralogical Society of America, Washington

Harrison TM (1981) Diffusion of ^{40}Ar in hornblende. Contrib Miner Petrol 78:324–331

Harrison TM, Duncan I, McDougall I (1985) Diffusion of ^{40}Ar in biotite; temperature, pressure and compositional effects. Geochim Cosmochim Acta 49:2461–2468

Houshi T, Bowring SA (1991) Lead isotopic heterogeneities within alkali feldspars: implications for the determination of initial lead isotopic compositions. Geochim Cosmochim Acta 55:2309–2316

Jaffey AH, Flynn KF, Glendenin LE, Bentley WC, Essling AM (1971) Precision measurement of half-lives and specific activities of ^{235}U and ^{238}U. Phys Rev C4:1889–1906

Joesten R (1992) Grain-boundary diffusion kinetics in silicate and oxide minerals. In: Ganguly J (ed) Diffusion, atomic ordering, and mass transport, vol 8. Springer, Berlin Heidelberg New York, pp 345–395

Krogh TE (1973) A low contamination method for hydrothermal decomposition of zircon and extraction of U and Pb for isotopic age determination. Geochim Cosmochim Acta 37:485–494

Krogh TE (1982) Improved accuracy of U–Pb zircon ages by the creation of more concordant systems using an air abrasion technique. Geochim Cosmochim Acta 46:637–649

Kunk MJ, Miller AP (2002) Completion of NIST calibration of argon spikes, and plans for interlaboratory calibration of MMhb-2. Geol Soc Amer Abs w Prog 34:340

Kunk MJ, Dalrymple GB, Snee LW (1994) Progress on the preparation of the proposed $^{40}Ar/^{39}Ar$ standard MMhb-1, plans for its calibration, and interlaboratory calibration of argon facilities. USGS Circ. In: Abstracts of the 8th international conference on geochronology, cosmochronology and isotope geology, 1107:183

Lee JKW, Onstott TC, Cashman KV, Cumbest RJ, Johnson D (1991) Incremental heating of hornblende in vacuo: implications for $^{40}Ar/^{39}Ar$ geochronology and the interpretation of thermal histories. Geology 19:872–876

Loferski PJ, Ayuso RA (1995) Petrography and mineral chemistry of the composite Deboullie pluton, northern Maine, USA.: implications for the genesis of Cu–Mo mineralization. Chem Geol 123:89–105

Lofgren G (1980) Experimental studies on the dynamic crystallisation of silicate melts. In: Hargraves RB (ed) Physics of magmatic processes vol. Princeton University Press, New Jersey, pp 487–551

Ludwig KR (1980) Calculation of uncertainties of U–Pb isotope data. Earth Planet Sci Lett 46:212–220

Ludwig KR (1991) Isoplot–a plotting and regression program for radiogenic isotope data. USGS Open-File report 91–445

Ludwig KR (1998) On the treatment of concordant uranium–lead ages. Geochim Cosmochim Acta 62(4):665–676

Mattinson JM (1973) Anomalous isotopic composition of lead in young zircons. Carnegie Inst Yearbook 72:613–616

Mattinson JM (1987) U–Pb ages of zircons: a basic examination of error propagation. Chem Geol 66:151–162

Mattinson JM (1994) Uranium decay constant uncertainties and their implications for high-resolution U–Pb geochronology. GSA Abstr Prog 77:A-221

Mattinson JM (2000) Revising the ''gold standard''—the uranium decay constants of Jaffey et al. 1971. Eos Trans. AGU, Spring Meet. Suppl., Abstract V61A–02

Mattinson JM (2003) CA (chemical abrasion)-TIMS: high-resolution U–Pb zircon geochronology combining high-temperature annealing of radiation damage and multi-step partial dissolution analysis. Eos Trans. AGU, Fall Meet. Suppl., Abstract V22E–06

Mattinson JM (2005) Zircon U–Pb chemical-abrasion (''CA-TIMS'') method: combined annealing and multi-step dissolution analysis for improved precision and accuracy of zircon ages. Chem Geol 220(1–2):47–56

McDougall I, Harrison TM (1999) Geochronology and thermochronology by the $^{40}Ar/^{39}Ar$ method, Oxford University Press, New York

Meurer WP, Boudreau AE (1996) An evaluation of models of apatite compositional variability using apatite from the Middle Banded series of the Stillwater Complex, Montana. Contrib Miner Petrol 125:225–236

Mezger K, Cosca MA (1999) The thermal history of the Eastern Ghats Belt (India) as revealed by U–Pb and $^{40}Ar/^{39}Ar$ dating of metamorphic and magmatic minerals: implications for the SWEAT correlation. Precam Res 1999:251–271

Mezger K, Rawnsley CM, Bohlen SR, Hanson GN (1991) U–Pb garnet, sphene, monazite, and rutile ages: implications for the duration of high-grade metamorphism and cooling histories, Adirondack, Mts., New York. J Geol 99:415–428

Min K, Mundil R, Renne PR, Ludwig KR (2000) A test for systematic errors in $^{40}Ar/^{39}Ar$ geochronology through comparison with U–Pb analysis of a 1.1 Ga rhyolite. Geochim Cosmochim Acta 64:73–98

Min K, Renne PR, Huff WD (2001) $^{40}Ar/^{39}Ar$ dating of Ordovician K-bentonites in Laurentia and Baltoscandia. Earth Planet Sci Lett 185:121–134

Mortensen JK, Roddick JC, Parrish RR (1992) Evidence for high levels of unsupported radiogenic ^{207}Pb in zircon from a granitic pegmatite: implications for interpretation of discordant U–Pb data. EOS, Trans Amer Geophys Union 73:370

Nemchin AA, Pidgeon RT (1999) U–Pb ages on titanite and apatite from the Darling Range granite: implications for Late Archean history of the southwestern Yilgarn Craton. Precam Res 96:125–139

Oberli F, Meier M, Berger A, Rosenburg CL, Giere R (2004) U–Th–Pb and $^{230}Th/^{238}U$ disequliibrium isotope systematics: precise accessory mineral chronology and melt evolution tracing in the Apline Bergell intrusion. Geochim Cosmochim Acta 68:2543–2560

Olson JC, Marvin RF, Parker RL, Mehnert HH (1977) Age and tectonic setting of lower Paleozoic alkalic and mafic rocks, carbonatites and thorium veins in south-central Colorado. Jour Res US Geol Survey Bull 5(6):673–687

Parker RL, Hildebrand FA (1963) Preliminary report on alkalic intrusive rocks in the northern Wet Mountains, Colorado. US Geol Survey Prof Paper 450-E:E8–E10

Parrish RR (1990) U–Pb dating of monazite and its application to geological problems. Can J Earth Sci 27:1431–1450

Pidgeon RT, Nemchin AA, Hitchen GJ (1998) Internal structures of zircons from Archean granites from the Darling Range batholith: implications for zircon stability and the interpretation of zircon U–Pb ages. Contrib Miner Petrol 132:288–299

Rasmussen B, Fletcher IR (2004) Zirconolite: a new U–Pb chronometer for mafic igneous rocks. Geology 32(9):785–788

Reid MR, Coath CD (2000) In situ U–Pb ages of zircons from the Bishop Tuff: no evidence for long crystal residence times. Geology 28:443–446

Reid MR, Coath CD, Harrison TM, McKeegan KM (1997) Prolonged residence times for the youngest rhyolites associated with Long Valley caldera: ion microprobe dating of young zircons. Earth Planet Sci Lett 150:27–38

Renne PR (2000) $^{40}Ar/^{39}Ar$ age of plagioclase from Acapulco meteorite and the problem of systematic errors in cosmochronology. Earth Planet Sci Lett 175:13–26

Renne PR, Karner DB, Ludwig KR (1998a) Absolute ages aren't exactly. Science 282:1840–1841

Renne PR, Swisher CC, Deino AL, Karner DB, Owens TL, DePaolo DJ (1998b) Intercalibration of standards, absolute ages and uncertainties in $^{40}Ar/^{39}Ar$ dating. Chem Geol 145:117–152

Rex DC, Guise PG, Wartho J-A (1993) Disturbed ^{40}Ar–^{39}Ar spectra from hornblendes: Thermal loss or contamination. Chem Geol 103:271–281

Samson SD, Alexander JEC (1987) Calibration of the interlaboratory ^{40}Ar–^{39}Ar dating standard, MMhb–1. Chem Geol 66:27–34

Schmitz MD, Bowring SA (2001) U–Pb zircon and titanite sytematics of the Fish Canyon Tuff: an assessment of high-precision U–Pb geochronology and its application to young volcanic rocks. Geochim Cosmochim Acta 65(15):2571–2587

Schmitz MD, Bowring SA (2003) constraints on the thermal evolution of continental lithosphere from U–Pb accessory mineral thermochronometry of lower crustal xenoliths, southern Africa. Contrib Miner Petrol 144:592–618

Schmitz MD, Bowring SA, Ireland TR (2003) Evaluation of Duluth Complex anorthositic series (AS3) zircon as a U–Pb geochronological standard: new high-precision isotope dilution thermal ionization mass spectrometry results. Geochim Cosmochim. Acta 67(19):3665–3672

Schoene B, Crowley JL, Condon DC, Schmitz MD, Bowring SA (2006) Reassessing the Uranium decay constants for geochronology using ID-TIMS U–Pb data. Geochim Cosmochim Acta 70:426–445

Schärer U (1984) The effect of initial ^{230}Th disequilibrium on young U–Pb ages: the Makalu case, Himalaya. Earth Planet Sci Lett 67:191–204

Schön R, Winkler G, Kutschera W (2004) A critical review of experimental data for the half-lives of the uranium isotopes ^{238}U and ^{235}U. Appl Radiat Isot 60:263–273

Shawe DR, Parker RL (1967) Mafic-ultramafic layered intrusion at Iron Mountain, Fremont County, Colorado. US Geol Survey Bull 1251-A:A1–A20

Spell TL, McDougall I (2003) Characterization and calibration of $^{40}Ar/^{39}Ar$ dating standards. Chem Geol 198:189–211

Stacey JC, Kramers JD (1975) Approximation of terrestrial lead isotope evolution by a two-stage model. Earth Planet Sci Lett 26:207–221

Steiger RH, Jäger E (1977) Subcommission on Geochronology: convention on the use of decay constants in geo- and cosmochronology. Earth Planet Sci Lett 36:359–362

Verts LA, Chamberlain KR, Frost CD (1996) U–Pb sphene dating of metamorphism: the importance of sphene growth in the contact aureole of the Red Mountain pluton, Laramie Mountains, Wyoming. Contrib Miner Petrol 125:186–199

Villa IM, Grobéty B, Kelley SP, Trigila R, Wieler R (1996) Assessing Ar transport paths and mechanisms in the McClure Mountains hornblende. Contrib Miner Petrol 126:67–80

Willmore CC, Boudreau AE, Kruger FJ (2000) The halogen geochemistry of the Bushveld Complex, Republic of South Africa: implications for chalcophile element distribution in the lower and critical zones. J Petrol 41:1517–1539

York D (1969) Least-squares fitting of a straight line with correlated errors. Earth Planet Sci Lett 5:320–324